Fabrication and Characterization of Gas Sensor Based on Gr/PANI/ZnS Nanocomposite

Elaf Kareem Salman, Ghaida Salman Muhammed

University of Baghdad, College of science, Department of physics, Baghdad, Iraq.
Email: elaphkareem63@gmail.com

Gr/PANI thin film deposited on silicon and porous silicon by photoelectrochemical etching method and doped with (1, 3 and 5)wt% ZnS nanoparticles. Structural, morphological and optical properties of the nanocomposite were characterized by XRD, SEM, and UV-VIS spectroscopy. X-ray diffraction (XRD) was used to evaluate the quality and dimensions of the crystals of graphene, zinc sulfide, polyaniline. Defects and the morphology of the nanoparticles due to the nanocomposite process were evaluated by scanning electron microscopy (SEM). The broadening sharp peaks in the XRD patterns indicated the formation nanocrystalline phase of ZnS with a crystallite size of less than 50 nm. These results SEM showed the interaction between Graphene /polyaniline and ZnS nanoparticles. The UV-Vis spectrum of composites shows peak at 459.34 nm and a broad peak in the range 652 nm. The gas sensor measurements showed that the resistivity of P-type gas sensor increases and return decreases by NO2 oxidization gas but N-type sensor decrease and increases by NO2 oxidization gas and both them decreases by high operation temperature. The sensitivity of the gas sensor increases in most samples with increases doping ratios for ZnS NPs. The best sensor for NO2 gas was the sample Gr/PANI/ ZnS (3 wt%) which deposited on porous silicon with a sensitivity of 118 % at 150oC.

Keywords: Graphene, Polyaniline, ZnS, Nanocomposite, Gas sensor.

1. Introduction

Nanotechnology focuses on the development of materials, technologies, or structures that have a size between 1 and 100 nanometers in at least one dimension. Nanosensors represent one of the initial implementations of nanotechnology. Nanosensors refer to chemical or biological sensors that transmit information using nanomaterials [1, 2].Increasing concerns about environmental pollution are increasing the need for gas sensors in a wide range of applications. Metal oxide gas sensors are widely used to detect various gases [3]. Gas sensitivity is an inherent property of polyaniline (PANI), a conducting polymer. PANI's susceptibility to various environmental contaminants, including CO, SO_2, NH_3, and other greenhouse gases, is contingent upon the specific processing methods employed. Numerous scientists have created

PANI-based sensors using different nonmanufacturing methods and assessed the stability and quality of the results. The stability and environmental friendliness of PANI, its straightforward synthesis process, its straightforward doping-dedoping chemistry, and its inexpensive cost are further benefits [4-6]. One popular carbon-based single-layered two-dimensional substance is graphene [7-9]. It possesses an exceptional electron mobility of 20,000 $cm^2 V^{-1} s^{-1}$ at ambient temperature and a large specific surface area. Its carrier density is 1012 cm^{-2} and its resistivity is 10^{-6} Ω.cm. For gas and vapour sensing, its electrical, mechanical, and chemical qualities are particularly helpful [10,11]. Numerous researchers have effectively examined graphene–PANI composites. However, binding materials are typically utilized during the preparation phase, which complicates the system and interferes with electrical conductivity [12]. Two more techniques that are frequently utilized to prepare PANI graphenen nonocomposites are in situ polymerization and solution mixing. Chemical polymerization is used in in situ polymerization to change aniline into polyaniline in a graphene-containing media. To create PANI-graphenecomposites, a straightforward technique called solution mixing is used, along with continuous stirring or ultra-sonication[13,14]. A composite is made up of several different materials; its properties can be entirely new or a weighted average of the constituent parts. The many uses of the GR/PANI nanocomposite are covered in recent studies, along with its structural, optical, thermal, and electrical characteristics [15-19]. In this work, we have examined how the optical shape and characteristics of the GR/PANI polymer are affected by changes in ZnS nanoparticle concentration. In order to ascertain the impact of the inorganic nanoparticle additives and the potential of the obtained hybrid materials to be useful for developing functional materials for nanoelectronics devices that have the dual advantages for room-temperature applications, the obtained hybrid materials were examined for their structural, optical, and morphological properties. It was discovered that the optical characteristics of these hybrid

2. Experimental work

2.1 Synthesis of GR/PANI/ ZnS Nanoparticles

To fabricate the sensor in this study, we followed the following steps: First, the nanocomposite was prepared by taking weight ratios of graphene and polyaniline dissolved in 50ml dimethyl formamide (DMF). Secondly, the compound prepared from GR/PANI was prepared with (7:3) formulations, and a sonication was issued in 10 min. Third, prepare zinc sulfide (ZnS) nanoparticles by mixing two chemical solutions with a concentration of 0.1M. The first solution was prepared by dissolving 1.36 g of zinc chloride powder ($ZnCl_2$) in 100 ml of distilled water. To adjust the pH, we added sodium hydroxide to the mixture at the power of 8. The pH controls the reaction rate due to the effect of the common ion. As for the second solution, we obtain it by dissolving 0.78 g of sodium sulfide powder (Na_2S) in 100 ml of distilled water. The two solutions stir at room temperature with a continuous flow of argon gas until ZnS nanoparticles are formed according to the following chemical reaction [20]:

$$ZnCl_2 + Na_2S \rightarrow ZnS + 2NaCl \quad \ldots\ldots\ldots\ldots\ldots\ldots (1)$$

Fourthly, addition of zinc sulfide (Zns) nanoparticles in different ratios (0.01,0.03 and 0.05) for the compound (GR / PANI).Fifthiy, Gr/PANI nanocomposite and doped with (0.01,0.03

and 0.05) ZnS NPs deposited on silicon and porous silicon by photoelectrochemical etching method.

3. Results and discussion

3.1 X-Ray Diffraction (XRD)

The X-ray diffraction pattern (XRD) of GR, GR/PANI and GR/PANI/ZnS NPs with different ratios of ZnS NPs were studied, as shown in figure (1).Figure (1a) illustrates the pristine graphene (XRD) peaks observed at 26.49° and 54.63°, which correspond to the hexagonal lattice of (002) and (004) planes [21,22]. The primary peaks are located at 26.49° and 54.63°, indicating basal spacings of d002= 3.36 Å and d004=1.67 Å, respectively. In the XRD analysis of the GR/PANI composites depicted in figure (1b), the X-ray diffraction pattern of polyaniline displays peaks at 11.7°, 16.4°, 21.2°, 21.3°, and 23.6°, along with a peak for graphene at 26.5°. These findings align with existing research [23,24 and 25].For the GR/PANI/ZnS NPs nanocomposites with different weights addition ratios (1,3, 5)wt% of ZnS NPs , a phase appeared for ZnS NPs with a cubic structure. At the same time, the peaks of GR/PANI/ZnS NPs at (1wt %) is appeared in figure (1c) when adding more ratios of ZnS NPs, the ZnS NPs peaks is high lighted as shown in figure (1d,f).The addition of high ratios of ZnS NPs activates the presence of cubic phase ZnS NPs. Table (1) displays information on the peak positions and miller indices for the diffracted planes, as well as the full width at half maximum and crystallite size.

The interplaner spacing d is calculated using the relation [26]:

$D_{hkl} = n\lambda / 2\sin\Theta$…….(2)

where λ is the X-ray wavelength (here λ = 1.54184 Å) and θ is the Bragg angle.

The average crystallite size is calculated from Scherer formula [27]:

$D=0.9\lambda/(\beta \cos\theta)$ ……....(3)

when measured in radians, β represents the full-width at half-maximum. Variations in the ZnS NP ratio are shown in Table (1) together with the XRD characteristics of GR, GR/PANI, and GR/PANI/ZnS NPs.

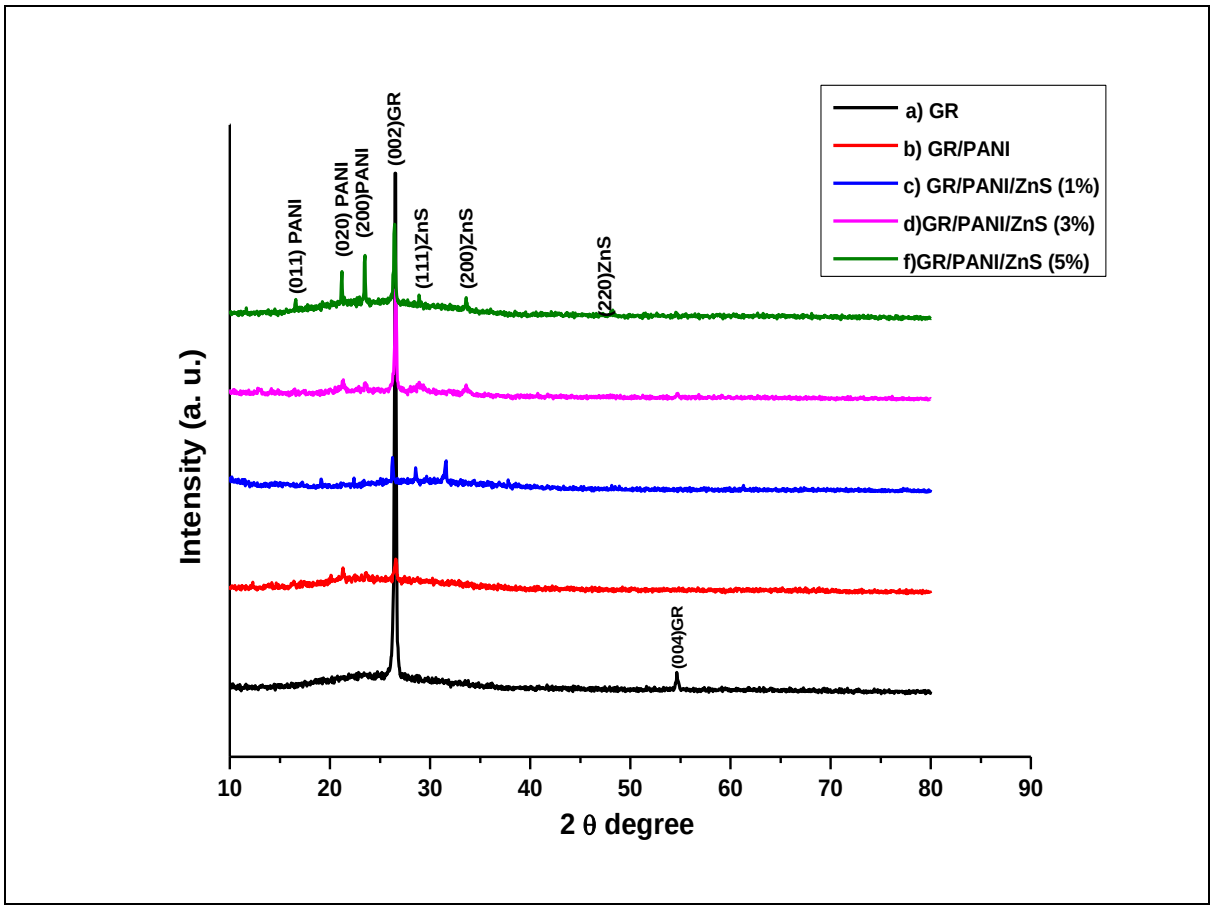

Figure 1: XRD spectra of the (a)GR, (b)GR/PANI, (c) GR/PANI/ZnS (1 wt%) nanocompsite, (d)GR/PANI/ZnS (3 wt%) nanocompsite and (f)GR/PANI/ZnS (5 wt%) nanocompsit.

Table 1: XRD parameters of the GR, GR/PANI and GR/PANI/ZnS NPs composites with different ratios of ZnS NPs

Sample	2θ (Deg.)	FWHM (radian)	d_{hkl} (Å)	C.S (nm)	Phase	(hkl)
GR	26.498	0.236	3.36	34.6	GR	(002)
	54.636	0.371	1.67	24.1	GR	(004)
GR/PANI	16.402	0.462	5.3999	17.4	PANI	(011)
	21.311	0.249	4.1660	32.5	PANI	(020)
	23.623	0.285	3.7632	28.5	PANI	(200)
	26.575	0.320	3.3515	25.5	G	(002)
	21.240	0.213	4.1798	37.9	PANI	(020)
GR/PANI/ZnS(1wt%)	23.552	0.178	3.7744	45.6	PANI	(200)
	26.575	0.213	3.3515	38.3	G	(002)
	21.347	0.285	4.1591	28.4	PANI	(020)
	23.552	0.285	3.7744	28.5	PANI	(200)
GR/PANI/ZnS(3wt%)	26.540	0.213	3.3559	38.2	G	(002)

	28.923	0.356	3.0846	23.1	Cub. ZnS	(111)
	33.618	0.462	2.6637	17.9	Cub. ZnS	(200)
	16.616	0.178	5.3310	45.2	PANI	(011)
	21.204	0.178	4.1867	45.5	PANI	(020)
	23.516	0.178	3.7800	45.6	PANI	(200)
GR/PANI/ZnS(5wt%)	26.469	0.249	3.3647	32.8	G	(002)
	28.887	0.178	3.0883	46.1	Cub. ZnS	(111)
	33.618	0.213	2.6637	38.9	Cub. ZnS	(200)
	48.095	0.285	1.8904	30.6	Cub. ZnS	(220)

3.2. Scanning Electron Microscopy (SEM)

Scanning electron microscopy (SEM) is a versatile technique for studying morphology of materials. The nanoparticle sizes were computed using the SEM Images. Figure (2a) illustrates the dispersion of (GR), which have nanosheets shape. The images of pure ZnS NPs, as shown in figure (2b), which prepared without adding the (GR/PNAI) has nanosize with nanoparticle structure. For the (GR/PNAI) SEM images prove the formation of nanocomposite, as shown in figure (2c) with diameter less than 100 nm. GR/PNAI /ZnS NPs with different ratios of ZnS NPs powder, are shown in figure (2d, e and f). It is clear that ZnS NPs are loaded on (GR/PNAI) nanosheet. It indicates that the ZnS NPs successfully penetrated the surrounding regions GR/PANI matrix [28]. The decrease of the diameter size at increased ratios of ZnS NPs, causing a relative decrease in the contents of GR/PANI nanocomposite because nanoparticles have little mass and large surface area [29].The average sizes of the GR/PNAI /ZnS nanocomposite with different ratios of ZnS NPs shown in Table (2).

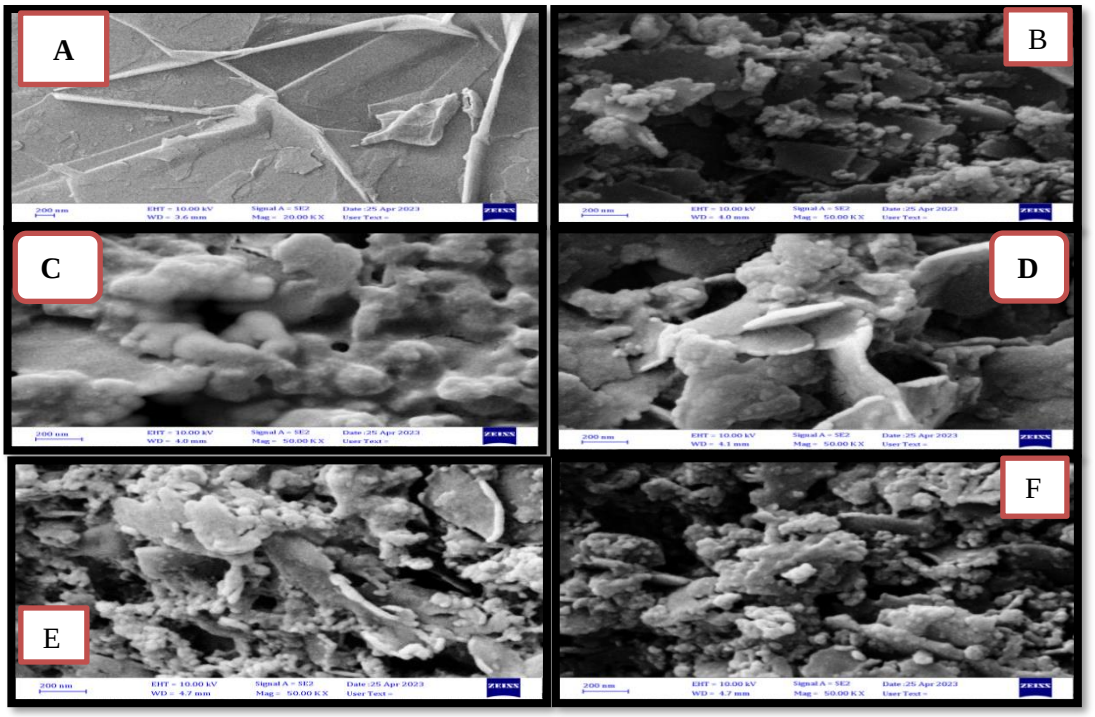

Figure 2: SEM images of (a) GR, (b) ZnS NPs , (c) GR/PANI nanocompsite, (d)

GR/PANI/ZnS (1 wt%) nanocompsite, (e)GR/PANI/ZnS (3 wt%) nanocompsite and (f)GR/PANI/ZnS (5 wt%) nanocompsite

Table 2: The average sizes of the GR, ZnS NPs, GR/PNAI and GR/PNAI /ZnS nano composite with different ratios of ZnS NPs .

Samples	Average Size (nm)
GR	68.081
ZnS	29.248
GR/PARI	44.939
GR/PANI/0.01 ZnS NP_s	35.596
GR/PANI/0.03 ZnS NP_s	30.486
GR/PANI/0.05 ZnS NP_s	26.796

3.3. UV-VIS absorption spectrum

Figure (3) illustrates the UV–VIS absorption spectra of GR/PANI, ZnS, and GR/PANI/ZnS NPs (1, 3, and 5) wt%. The spectra reveal a distinct absorption peak at approximately 459.34 nm and a broad absorption around 652 nm. The 459.34 nm absorption band is attributed to π–π* transition, while the 652 nm absorption band is associated with the quinoid ring transition within the polyaniline chain. This finding aligns with previous research conducted by [30].

Where transmittance (T) is given by ratio of the intensity of the light (IT) transmitting through the film to the intensity of the incident light (I) as follows [31]:

$T=I_T/I$…… (4)

Where:

T: transmittance.

I_T: transmitted light intensity.

I: light intensity.

The absorbance of the sample is defined as the negative log of the transmittance given by the relation [32]:

$A = -\log_{10} T$ …… (5)

Where

A: the absorbance of the sample.

When ZnS nanoparticles were added to GR and PANI in the GR/PANI/ZnS nanocomposite, the ZnS nanoparticles' wavelength increased. When tiny particles aggregate and consolidate, the bands amplify a more complicated growth mechanism [33,34]. This finding is consistent with previous findings reported by [30].

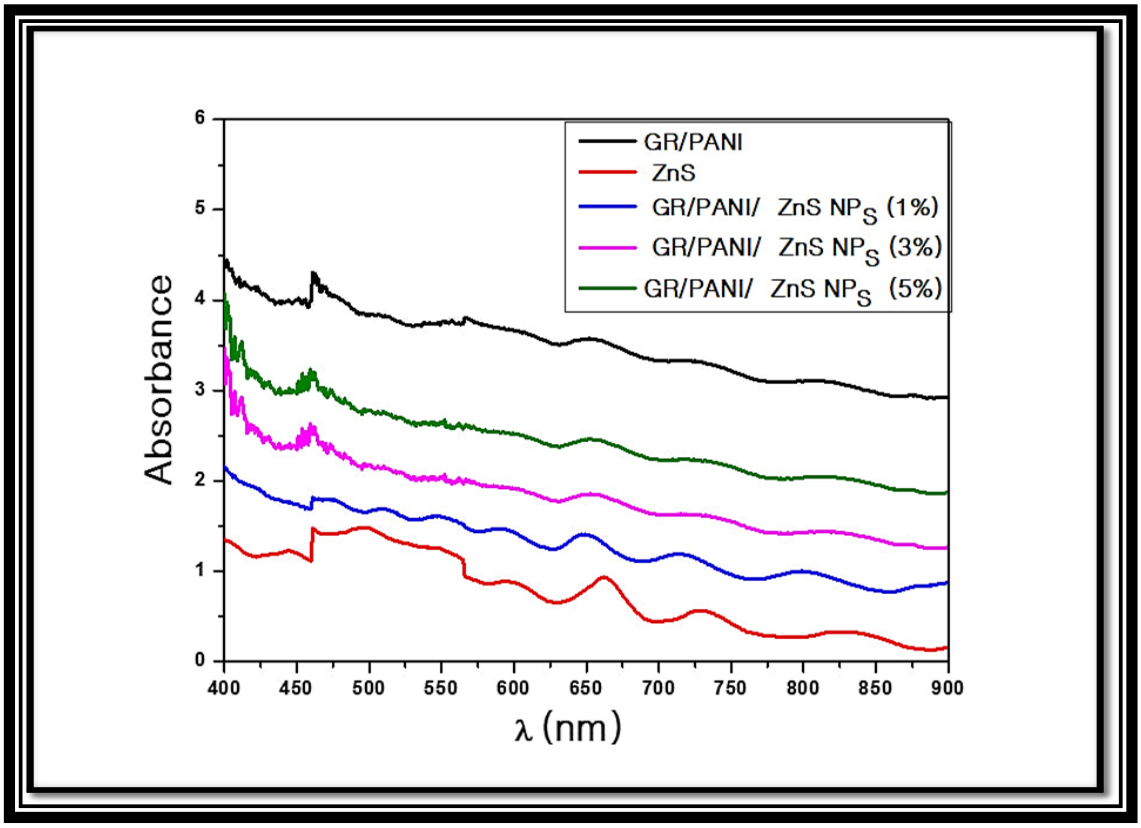

Figure 3: UV–Vis absorption spectra of the ZnS, GR/PNAI and GR/PNAI /ZnS nano composite with different ratios of ZnS NPs

The fundamental absorption, which corresponds to the transition from the valence band to the conduction band, can be used to determine the band gaps of the materials by utilizing Tauc relation shown in equation (6) [35].

$\alpha h\upsilon = A(h\upsilon - Eg)^n$……(6)

Plots of $(\alpha h\upsilon)^2$ versus the photon energy ($h\upsilon$) in the absorption region near the fundamental absorption edge indicate the direct allowed transition for all samples as shown in Figure (4)

The energy gap values for graphene/polyaniline were determined to be 2.06ev and for zinc sulfide to be 1.88ev.

It has been observed that the energy gap values after adding ZnS at different ratios (1,3 and 5) wt % to GR/PANI, the optical energy gap decreased from 2.06ev to 1.89ev then to 1.5 ev and 1.4ev due to the chemical bonding of graphene and ZnS nanoparticles and this variation indicates that the electronic properties of ZnS nanoparticles are strongly modified by the presence of graphene and provide more electrical conductivity in the composite [36].

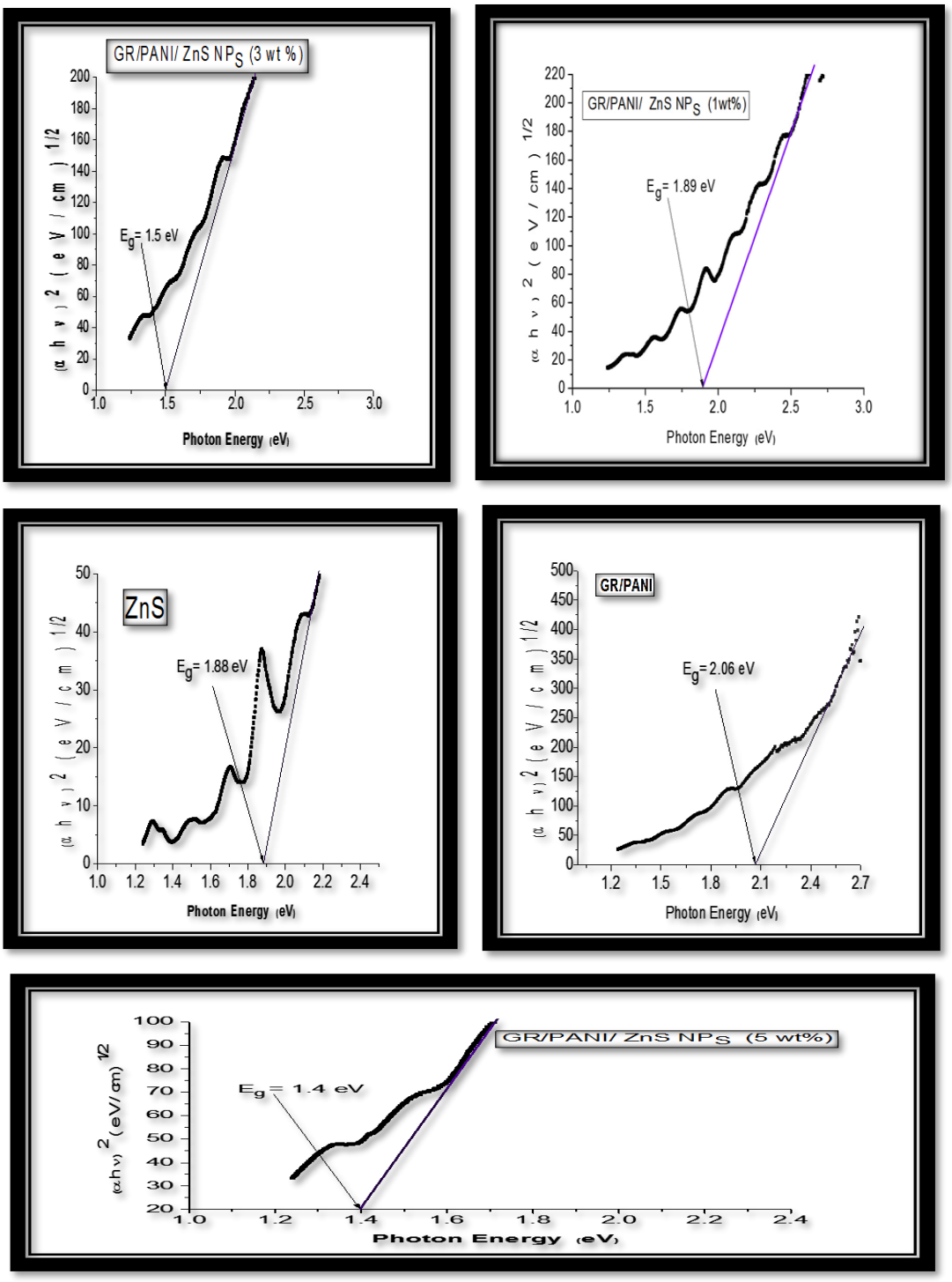

Figure (4): Energy Band gap of of the GR/PNAI ,ZnS and GR/PNAI /ZnS nanocomposite

with different ratios of ZnS NPs

Table (3): Energy Band gap of all samples calculated using the Tauc relationship equation (6).

Samples	Energy gap (ev)
GR/PANI	2.06
ZnS	1.88
GR/PANI/ZnS(1wt%)	1.89
GR/PANI/ZnS(3wt%)	1.5
GR/PANI/ZnS(5wt%)	1.4

3.4. Hall Effect

Hall effect measurement is used to determine the hall mobility (μH), carrier concentration (nH) and majority of electrical carriers type for all samples at different ratio. The variation of carriers concentration (nH) and hall mobility (μH) are shown in Table (4). From the Table, it was clear that the carrier concentration increases and carrier mobility (μH) decreases with doping ratio in case deposition on porous silicon, while noticed there was a decrease in carrier concentration and increases in carrier mobility (μH) with doping ratio in case deposition on normal silicon this is due to decreasing the disorders of the crystal lattice, which causes a decrease in phonon scattering and ionized impurity scattering and results in a decrease in mobility [37].Hall parameters of Gr/PANI andGr/PANI/ZnS NPs (1, 3 and 5)wt% deposited on porous silicon and silicon shown in Table (4).

Table (4): Hall parameters of GR/PANI andGR/PANI/ZnS NPs (1, 3 and 5) wt% deposited on silicon and pours silicon

Samples	$R_H(cm^{-3}\ c^{-1})$	Concentration (cm^{-3})	Mobility ($cm^2/v.s$)	Conductivity $(\Omega.cm)^{-1}$	Type
GR/PANI/PS	6.94×10^{2}	8.99×10^{15}	1.10×10^{3}	1.59	P
GR/PANI/ZnS NPs at (1wt)/PS	5.87×10^{2}	1.06×10^{16}	8.28×10^{2}	1.41	P
GR/PANI/ZnS NPs at (3wt)/PS	1.37×10^{3}	4.55×10^{15}	1.35×10^{3}	9.86×10^{-1}	P
GR/PANI/ZnS NPs at (5wt)/PS	2.27×10^{2}	2.76×10^{16}	4.17×10^{2}	1.84	P
GR/PANI/Si	-2.53×10^{3}	-2.47×10^{15}	3.53×10^{3}	1.40	N
GR/PANI/ZnS NPs at (1wt)/Si	1.29×10^{3}	4.84×10^{15}	7.26×10^{2}	5.63×10^{-1}	P
GR/PANI/ZnS NPs at (3wt)/Si	-4.86×10^{2}	-1.28×10^{16}	9.82×10^{2}	2.02	N
GR/PANI/ZnS NPs at (5wt)/Si	1.49×10^{2}	4.19×10^{16}	3.86×10^{2}	2.59	P

3.5. Gas Sensing measurements of Gr/PANI and Gr/PANI/ZnS deposited on porous silicon toward NO2 gas

The variation of resistance as a function of time is shown in figure (5). The films specimens are examined for gas sensing using NO2 gas at a mixing ratio of 1:9, NO2: air.NO2/ with concentration of 86.123 ppm at different operation temperatures, 25, 100,150, and 200 ^{o}C,

resistance fluctuation was measured as a function of time. The resistance decreases with operating temperatures, when exposure to NO2. The metal oxides semiconductors can be divided into n- and p-type, which exhibited different sensing behavior to the same detecting gas. Upon exposure to oxidizing gases, the gas species act as acceptors, leading to resistance increase for n-type semiconductor and decrease for p-type semiconductor.

As for the reducing gases, the gas species act as donors, leading to resistance decrease for n-type semiconductor and increase for p-type semiconductor [38]. It was found that a high working temperature reduced the sensor's resistance as the Figure (5) where the resistance decreases .This occurs because more valence band electrons depart as the temperature rises and join the conduction band, boosting conductivity.

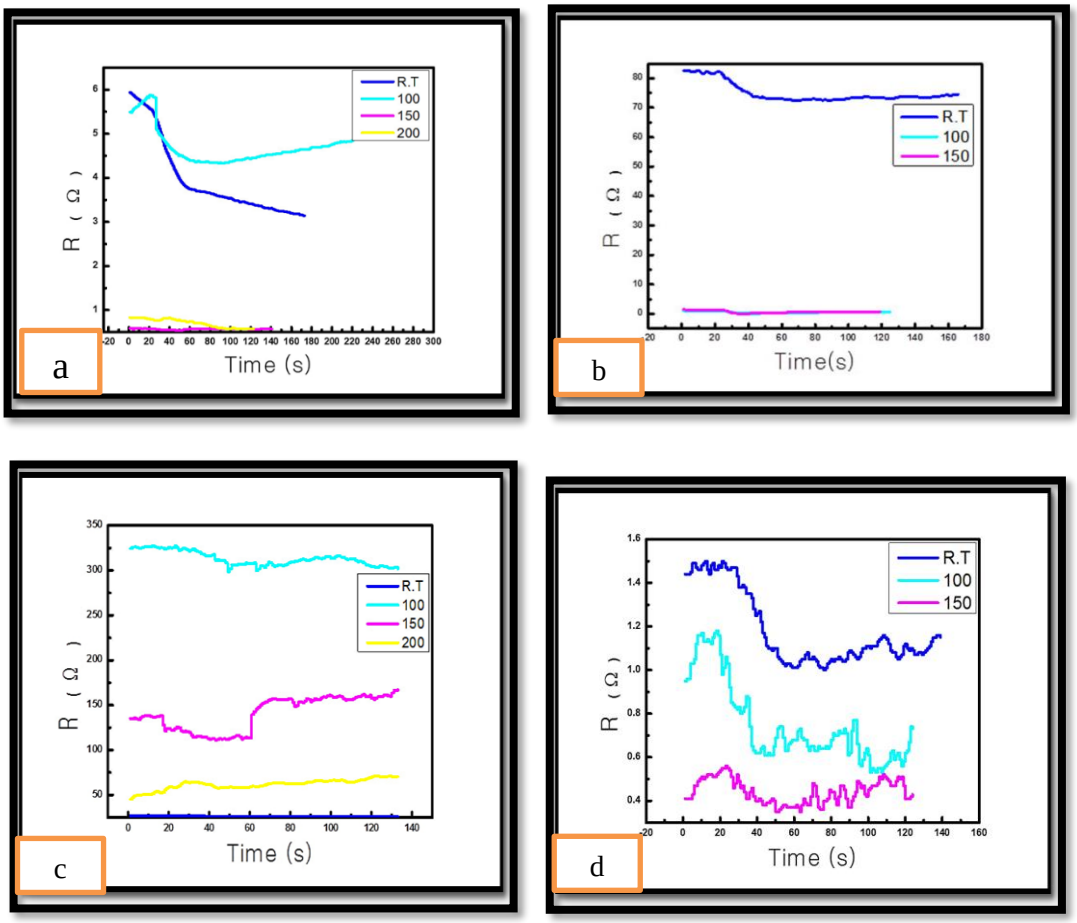

Figure(5): The variation of resistance with time toward NO2 gas at (25,100,150 and 200ºC)for (a)GR/PANI (b)Gr/PANI/ ZnS NPs (1wt%) (c) Gr/PANI/ ZnS NPs (3wt%) (d) Gr/PANI/ ZnS NPs (5wt%) deposited on porous silicon substrate.

The figure (6), show the sensitivity(S%) of GR/PANI and GR/PANI/ZnS NPs (1, 3 and 5)wt% where increases with operating temperature of all sensor cell. The maximum sensitivity of GR/PANI of 95% was obtained at 150°C testing temperature. While the maximum

sensitivity of GR/PANI/ZnS NPs (1wt%) of 27% was obtained 25°C testing temperature then which it began to drop with increasing T. As for the maximum sensitivity of GR/PANI/ZnS NPs(3wt%) of 118% was obtained at 150°C testing temperature then which it began to drop with increasing T. While the high sensitivity of GR/PANI/ZnS NPs (5wt%) of 48% at 100 °C testing temperature then which it began to drop with increasing T. It can be seen that sensitivity increases with operating temperature of most sensor cell because decreasing the grain size and increases the surface area [39].

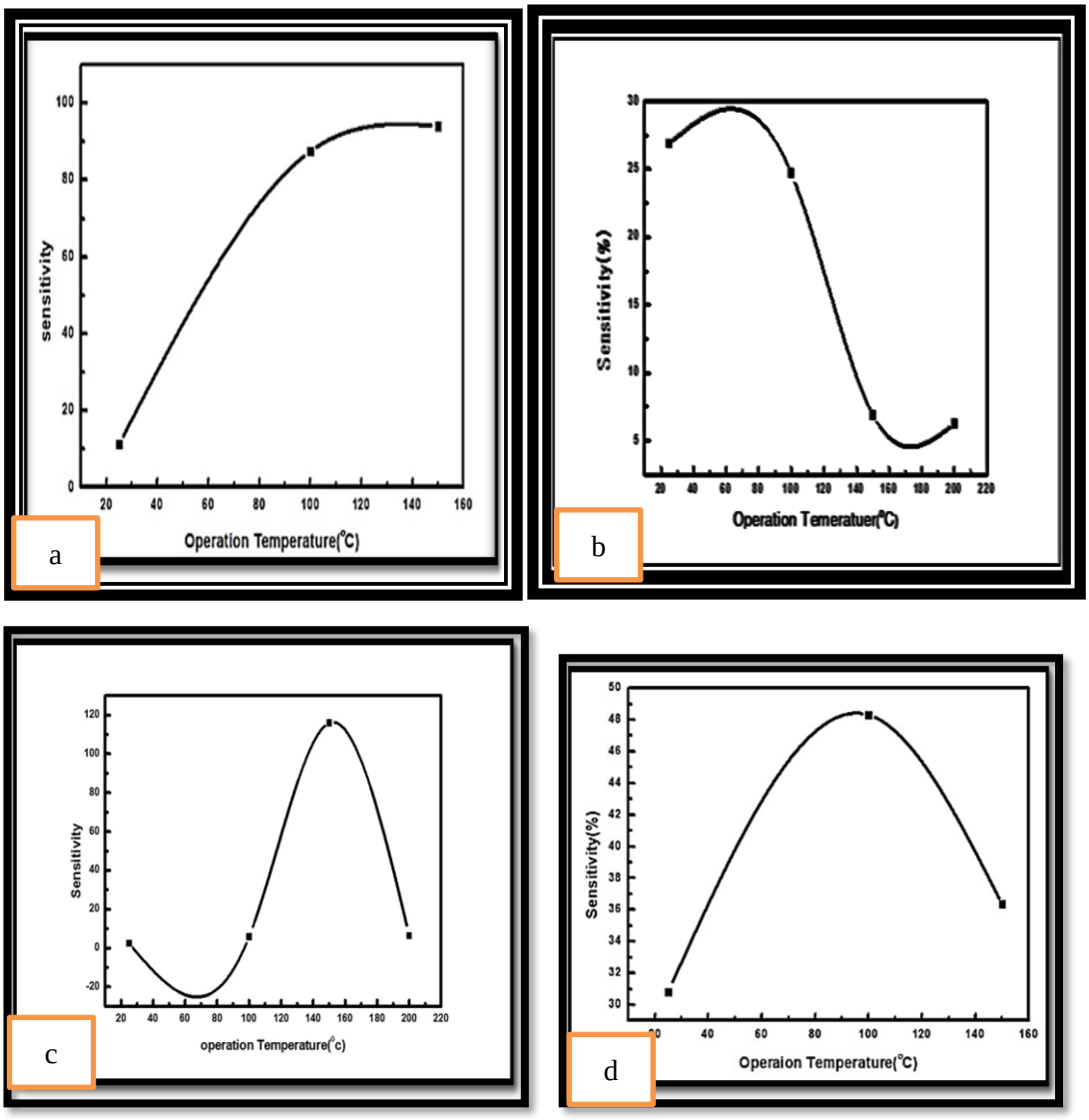

Figure (6): The sensitivity of (a)GR/PANI (b)GR/PANI/ ZnS NPs (1wt%) (c) GR/PANI/ ZnS NPs (3wt%) (d) GR/PANI/ ZnS NPs (5wt%) deposited on porous silicon substrate.

Figure (7) show the response and recovery times of the gas sensor in the presence of NO2 at various temperatures. The reaction time is obviously sped up by adding ZnS NPs to

the host material, especially at higher doses. Due to the gas sensor cell's crystal structure. The dynamic times of the gas sensor cell are not too long. Rapid mass transfer of NO2 molecules into and out of the sensor as well as improved charge carrier mobility are made possible by this structure [40]. The following process governs the chemical adsorption of NO2 gas, which is the basic of the sensor mechanism. Due to faster gas diffusion, response and recovery periods shorten as temperature increases [40]. Table (5), show the sensitivity, response and recovery time for GR/PANI and GR/PANI/ZnS NPs (1, 3 and 5) wt% deposited on porous silicon upon exposure to the NO2 gas.

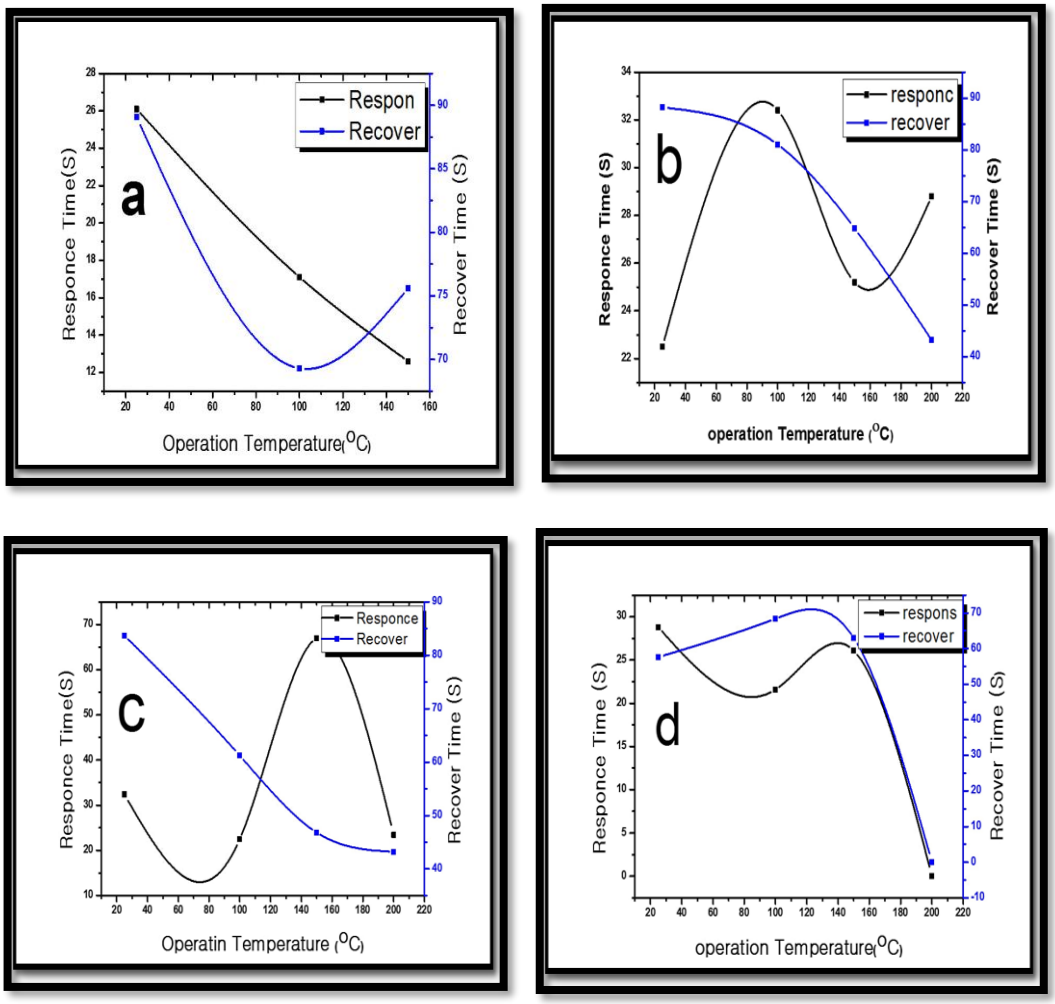

Figure (7): Response and recovery time of: (a)GR/PANI (b)GR/PANI/ ZnS NPs (1wt%) (c) GR/PANI/ ZnS NPs (3wt%) (d) GR/PANI/ ZnS NPs (5wt%) deposited on porous silicon substrate.

Table (5): The sensitivity, response and recovery time of GR/PANI and GR/PANI/ZnS NPs (1,3 and 5)wt% deposited on porous silicon upon exposure to NO2 gas at different operating temperature.

Type	T(˚C)	S %	t_s (s)	t_c (s)
GR/PANI/PS	25	10	26	89
	100	85	17	69
	150	95	13	75
GR/PANI/ZnS NPs (1wt%)/PS	25	27	22	88
	100	25	32	81
	150	7	25	65
	200	6	28	43
GR/PANI/ZnS NPs (3wt%)/PS	25	4	33	84
	100	6	23	61
	150	118	66	47
	200	6	23	43
GR/PANI/ZnS NPs (5wt%)/PS	25	31	28	58
	100	48	22	68
	150	36	26	63
	200	/	0	0

3.6. Gas Sensing measurements of Gr/PANI and Gr/PANI/ZnS deposited on silicon toward NO2 gas

Figure (8), shows the variation of resistance as a function of time for the samples deposited on silicon. The specimens are examined for gas sensing using NO2 gas at a mixing ratio of 1:9, NO2: air.NO2 with concentration of 86.123 ppm at different operation temperatures, 25, 100 , 150 and 200 ºC, resistance fluctuation was measured as a function of time. The resistance decreases with operating temperatures, when exposure to NO2. Metal oxide semiconductors can be categorized into n-type and p-type, each demonstrating distinct sensing responses to the same target gas. When in contact with oxidizing gases, these gases function as acceptors, resulting in an increase in resistance for n-type semiconductors and a decrease in resistance for p-type semiconductors .

As for the reducing gases, the gas species act as donors, leading to resistance decrease for n-type semiconductor and increase for p-type semiconductor [38]. It was found that a high working temperature reduced the sensor's resistance as the figure (8), where the resistance decreases. This occurs because more valence band electrons depart as the temperature rises and join the conduction band, boosting conductivity.

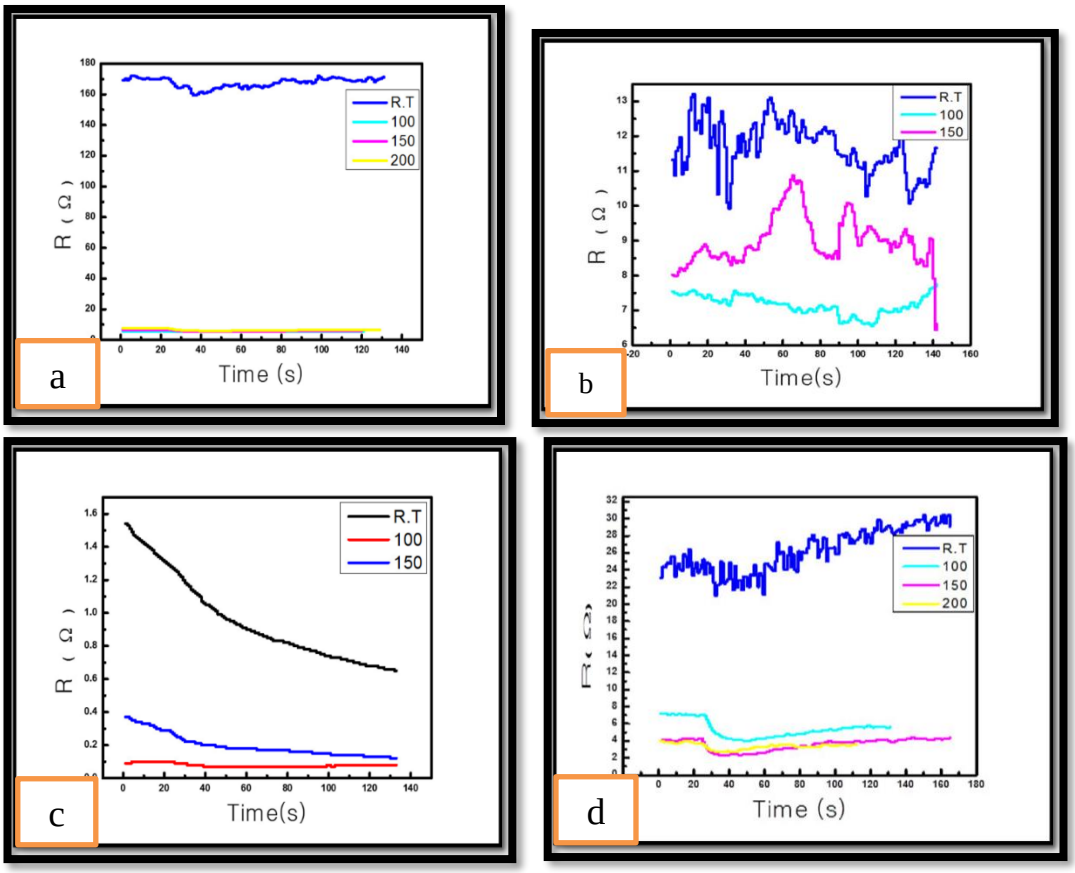

Figure (8): The variation of resistance with time toward NO2 gas at (25,100,150 and 200 ^{o}C)for (a)GR/PANI (b)GR/PANI/ ZnS NPs (1wt%) (c) GR/PANI/ ZnS NPs (3wt%) (d) GR/PANI/ ZnS NPs (5wt%) deposited on silicon substrate.

Figure (9) illustrates the sensitivity of GR/PANI and GR/PANI/ZnS NPs (1, 3 and 5) wt%, which increases with the operating temperature of the sensor device. The maximum sensitivity of GR/PANI, reaching 45%, was achieved at a testing temperature of 150°C, beyond which it started to decrease as the temperature rose. Conversely, the maximum sensitivity of GR/PANI/ZnS NPs (1wt %) was 4.7% at a testing temperature of 25°C, decreasing with higher temperatures. Similarly, the maximum sensitivity of GR/PANI/ZnS NPs (3wt%) was recorded at 38% at a testing temperature of 150°C. Moreover, the high sensitivity of GR/PANI/ZnS NPs (5wt%) was observed to be 23% at a testing temperature of 200°C.

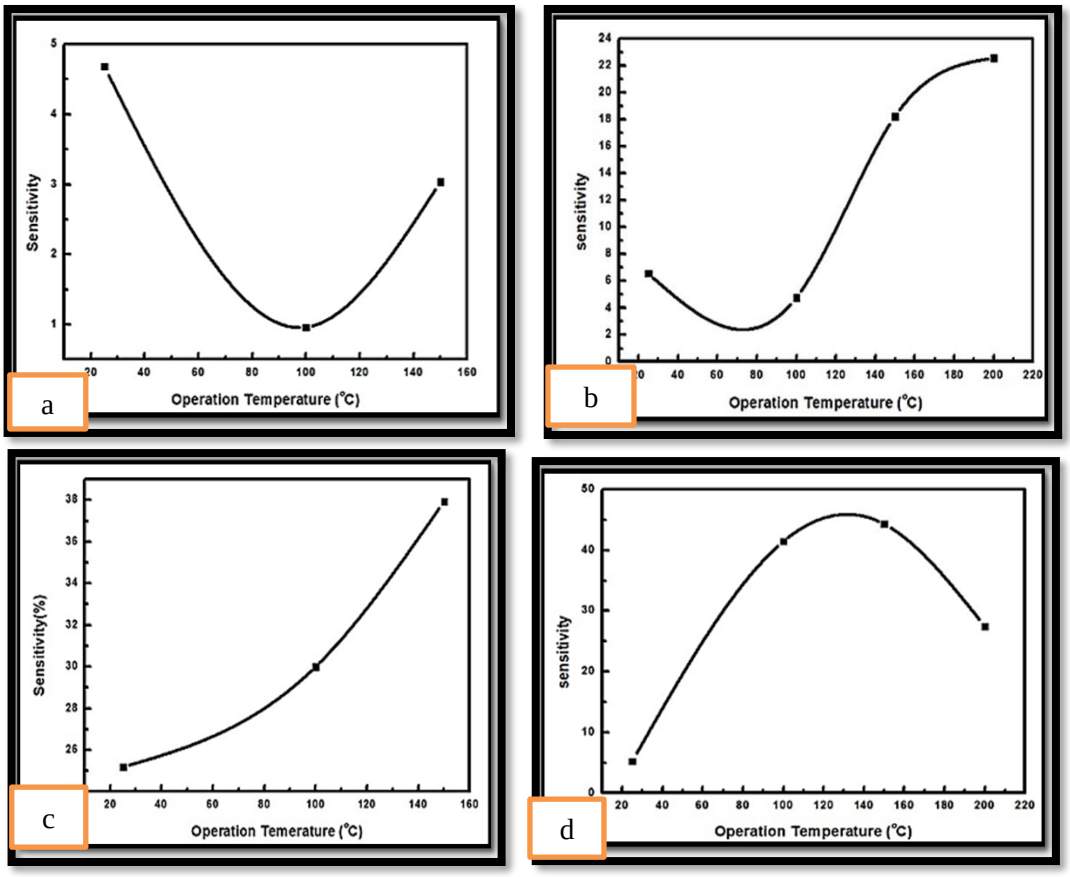

Figure (9): The sensitivity of (a)GR/PANI (b)GR/PANI/ ZnS NPs (1wt%) (c) GR/PANI/ ZnS NPs (3wt%) (d) GR/PANI/ ZnS NPs (5wt%) deposited on silicon substrate.

For figures (6) and (9), it can be seen that the sensitivity of the GR/PANI/PS is 95% at 150˚C higher than the GR/PANI/Si that equal 45% at 150℃. While GR/PANI/ZnS NPs (1wt%)/PS is 27% at 25˚C higher than the GR/PANI/ZnS NPs (1wt%)/ Si that equal 4.7% at 25˚C. As for the sensitivity of the GR/PANI/ZnS NPs (3wt%)/PS is 118% at 150˚C higher than the GR/PANI/ZnS NPs (3wt%)/ Si that equal 38% at 150˚C. While the sensitivity of the GR/PANI/ZnS NPs (5wt%)/PS is 48% at 100˚C higher than the GR/PANI/ZnS NPs (5wt%)/ Si that equal 23% at 200˚C, because decreasing the grain size and increases the surface area [39].

Figure (10), show the response and recovery times for the samples deposited on silicon in the presence of NO2 at various temperatures. The reaction time is obviously sped up by adding ZnS NPs to the host material, especially at higher doses. Due to the gas sensor cell's crystal structure. The dynamic times of the gas sensor cell are not too long. Rapid mass transfer of NO2 molecules into and out of the sensor as well as improved charge carrier mobility are made possible by this structure [40]. The following process governs the chemical adsorption of NO2 gas, which is the basic of the sensor mechanism. Due to faster gas diffusion, response and

recovery periods shorten as temperature increases [40]. Table (6), shows the sensitivity, response and recovery time for GR/PANI and GR/PANI/ZnS NPs (1, 3 and 5)wt % deposited on silicon upon exposure to the NO2 gas.

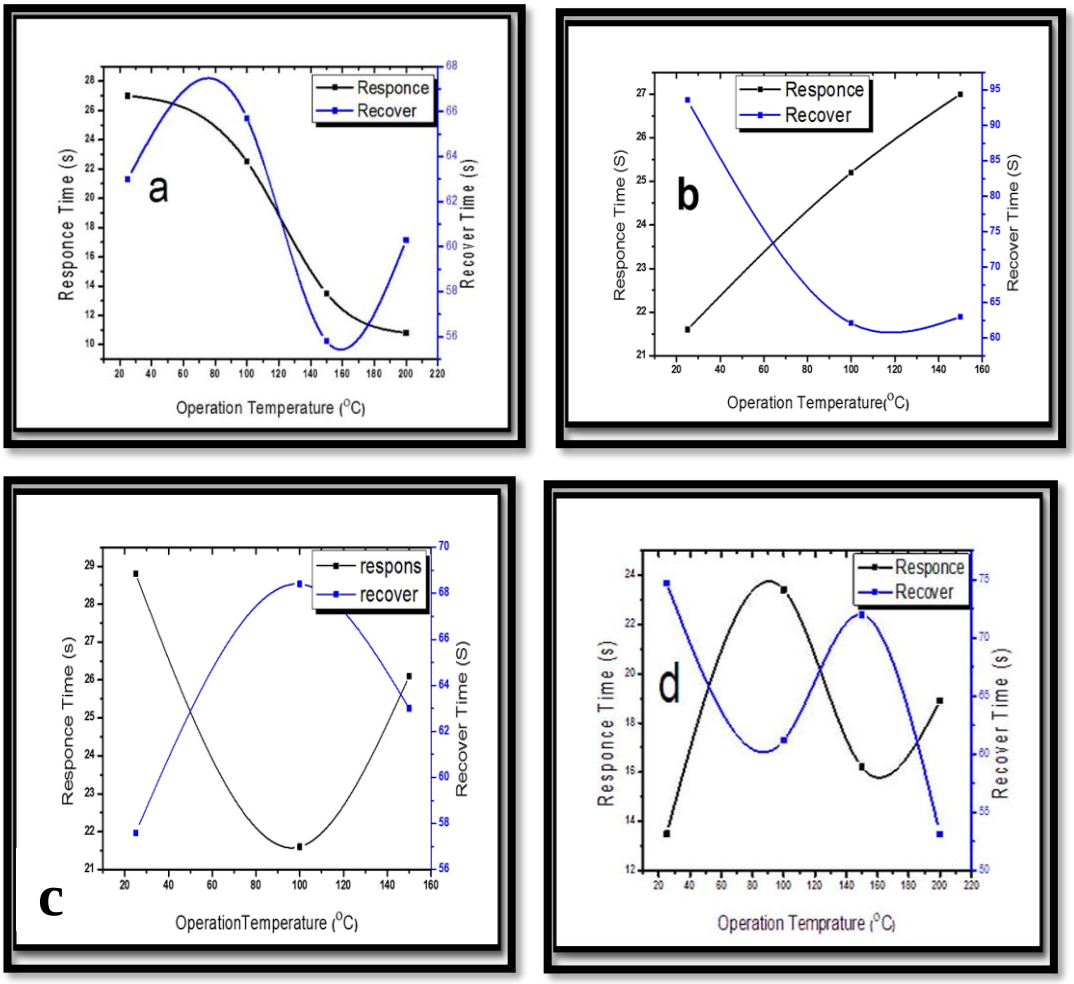

Figure (10): Response and recovery time of: (a)GR/PANI (b)GR/PANI/ ZnS NPs (1wt%) (c) GR/PANI/ ZnS NPs (3wt%) (d) GR/PANI/ ZnS NPs (5wt %) deposited on silicon substrate.

Table (6): The sensitivity, response and recovery time of GR/PANI and GR/PANI/ZnS NPs (1,3 and 5)wt% deposited on silicon substrate upon exposure to NO2 gas at different operating temperature.

Type	T(˚C)	S%	t_s(s)	t_c(s)
GR/PANI/Si	25	5	27	63
	100	40	23	66
	150	45	14	56
	200	27	11	60
GR/PANI/ZnS NPs (0.01)/	25	4.7	22	93

Si	100	1.1	25	62
	150	3.1	27	63
GR/PANI/ZnS NPs (0.03)/ Si	25	25	29	58
	100	30	22	68
	150	38	26	63
GR/PANI/ZnS NPs (0.05)/ Si	25	6.5	13	75
	100	5	23	61
	150	18	17	72
	200	23	19	53

4. Conclusions

1- Possibility preparing films from GR/PANI nanocomposite and GR/PANI/ZnS NPs (1, 3 and 5) wt % by chemical deposition method and these prepared films were deposited on silicon and porous silicon substrates by photoelectrochemical etching method.

2 -The Possibility of manufacturing a gas sensor from GR/PANI/ZnS NPs with high sensitivity by photoelectrochemical etching method .

3- The sensitivity of the gas sensor increases in most samples by adding ZnS NPs.

4- The best sensor performance for NO2 gas was for the sample GR/PANI/ ZnS NPs (3 wt%) which deposited on porous silicon with a sensitivity of 118 % at 150℃

Author Contributions: Each co-author has made unique contributions to the work. The author Elaf Kareem Salman prepared the Gr/PANI/ZnS nanocomposite, measured the gas sensor characteristics and contributed to writing the article draft and wrote the program for optical properties and contributed to the analysis of the results. As the author Ghaida Salman Muhammed, She supervised the work and reviewed the article draft.

Funding The authors have not disclosed any funding.

Data Availability Data sharing is not applicable to this article as no datasets were created or analyzed during the current study.

Declarations

Competing interests The authors have not disclosed any competing interests.

Ethical Approval The authors would like to declare that they do not have any conflict of interests.

References

1. Asama N Naje , and Waleed k Mahmood,"Sensitivity Performance of Single Wall Carbon Nanotubes Gas Sensor on Silicon and Porous Silicon", Materials Science and Engineering, Vol. 454, pp. 1-12, (2018).
2. Ali Eatemadi, Hadis Daraee, Hamzeh Karimkhanloo, Mohammad Kouhi,Nosratollah Zarghami,Abolfazl Akbarzadeh, Mozhgan Abasi, Younes Hanifehpour and Sang Woo Joo 2014 Carbon nanotubes: properties, synthesis, purification, and medical applications

Nanoscale Research Letters 9 393.
3. Sally K. Abbas and Asama N. Naje, "Enhancement of Functionalized Carbon Nanotubes Gas Sensor by Adding Metal Oxide Nanoparticles", Iraqi Journal of Physics, Vol.18, No.47, PP. 62-72, (2020).
4. A. Haynes and P. I. Gouma, Polyaniline-Based Environmental Gas Sensors, Sensors for Environment, Health and Security, 451–459 (2009)
5. J. Y. Shimano and A. G. MacDiarmid, Polyaniline, a dynamic block copolymer: key to attaining its intrinsic conductivity, Synth. Met., 123(2), 251–262 (2001)
6. W. Lyu, M. Yu, J. Feng and W. Yan, Highly crystalline polyaniline nanofibers coating with low-cost biomass for easy separation and high efficient removal of anionic dye ARG from aqueous solution, Appl. Surf. Sci., 458,413–424 (2018)
7. S. W. Ng, N. Noor and Z. Zheng, Graphene-based two dimensional Janus materials, NPG Asia Mater., 10, 217–237 (2018)
8. V. Singh, D. Joung, L. Zhai, S. Das, S. I. Khondaker and S. Seal, Graphene based materials: past, present and future, Prog. Mater. Sci., 56(8), 1178–1271 (2011)
9. M. I. Katsnelson, Graphene: carbon in two dimensions, Mater. Today, 10(1-2), 20–27 (2007)
10. S. Basu and P. Bhattacharyya, Recent developments on graphene and graphene oxide based solid state gas sensors, Sens. Actuators B: Chemical, 173, 1–21 (2001)
11. U. Latif and F. L. Dickert, Graphene Hybrid Materials in Gas Sensing Applications, Sensors, 15(12), 30504–30524 (2015)
12. Y. Li, Y. A. Samad, K. Polychronopoulou, S. M. Alhassan and K. Liao, Highly Electrically Conductive Nanocomposites Based on Polymer Infused Graphene Sponges, Sci. Rep., 4, (2014)
13. A. Kumar, V. Kumar, M. Kumar and K. Awasthi, Synthesis and characterization of hybrid PANI/MWCNT nanocomposites for EMI applications, Polym. Compos., 39(11), 3858-3868 (2018)
14. U. Male, S. Palaniappan and B. S. Singu, Incorporation of polyaniline nanofibres on graphene oxide by interfacial polymerization pathway for supercapacitor, Int. Nano Lett., 5(4), 231–240 (2015)
15. I. H. Kadhim, H. A. Hassan and Q. N. Abdullah, Hydrogen gas sensor based on nanocrystalline SnO2 thin film grown on bare Si substrates, Nano-Micro Lett., 8(1), 20-28 (2016)
16. C. Li and G. Shi, Three-dimensional graphene architectures, Nanoscale, 4(18), 5549-5563 (2012)
17. B. P- Lopez and A. Merkoçi, Nanomaterials based biosensors for food analysis applications, Trends Food Sci. and Technol., 22(11), 625-639 (2012)
18. J. Bhadra, A. Popelka, A. Abdulkareem, Z. Ahmad, F. Touatib and N. Al-Thani, Fabrication of polyaniline–graphene/polystyrene nanocomposites for flexible gas sensors, RSC Adv., 9(22), 12496-12506 (2019)
19. A. J. Burris, K. Tran, and Q. Cheng, Tunable Enhancement of a Graphene/Polyaniline/Poly(ethylene oxide) Composite Electrospun Nanofiber Gas Sensor, J. Anal. Test., 1(12), 1-10 (2017).
20. G. Salman, M. Medhat and A. Muhammed, "Effect of High pH Variation on the Structural and Optical Properties of ZnS Nanoparticles Prepared by Chemical Route", Australian Journal of Basic and Applied Sciences, Vol.11, No.7, p.p. 29-36, 2017.
21. F. E. Jorge, L. G. P. Tienne, M. D. V. Marques, Mat. Sci. and Eng. B, 263, 114-151, (2021).
22. A. R. Kachere, P. M. Kakade, A. R. Kanwade, P. Dani, N. T. Mandlik, S. R. Rondiya, N. Y. Dzade, S. R. Jadkar and Sh. V. Bhosale, ES Mater. Manuf., 16, 19-29, (2022).
23. A. U. Agobia, A. I. Ikeubac, A. J. Ekpunobia, I. L. Ikhioyad, K. I. Udofiaa, J. Effiom-Edem Ntibib , C. N. Ozoemenae, and M. A. Abua, Revista Mexicana de Fısica, 69, 1–9, (2023).
24. A. Alamgeer, M. Tahir, M. R. Sarker, S. Ali, I. Ibraheem, S. Hussian, S. Ali, M. I. Khan, D.

N. Khan, R. Ali and S. M. Said, Poly., 15, 3-63, (2023).
25. A. H. Mohammed, A. N. Naje and R. k. Ibrahim," photoconductive Detector Based on Graphene Doping with Silver Nanoparticles" ,Iraqi Journal of Science, 63, 5218–5231, (2022).
26. C. Kittel, "Introduction to Solid State Physics" , 7th Edition, John Weily and Sons Inc, Newyork, (1996).
27. L. Kernazhitsky, V. Shymanovska, T. Gavrilko, V. Naumov and V. Kshnyakin, "Optical Absorption of Polydisperse TiO2: Effect of Surface Doping by Transition Metal Cations", Ukrainian Journal of Physical Optics, Vol. 14, pp.15-23, (2013).
28. S. A. Khalaf and I. M. Ali, "Enhancement of NO2 gas sensing behavior for ZnS/PPy nanostructure by loading grapheme", Iraqi Journal of Physics, Vol.17, PP. 21-32, (2019).
29. M. Parmar, Ch. Balamurugan , D. Lee ," PANI and Graphene/PANI Nanocomposite Films — Comparative Toluene Gas Sensing Behavior", Sensors, Vol, 13:pp. 16611–16624, (2013).
30. M. Fauzi , Y. W. Fen, J. Abdullah, M. A. Kamarudin N. I.N. Alia, S. Omar, F. B. K. Eddin, N. S. M. Ramdzan and W. M. E. M. M. Daniyal, Photonics , 9, 300-310, (2022).
31. Himanshu Gupta, B.L.Chaudhary, Shameem Ahmad, K.P.Tiwari and P.A.Alvi. "Performance Analysis of AlGaN-LED for D-UV Emission".AIP Conference Proceedings, 2220, (2020):130008.
32. S. Al-Mgrs, Sh. Habeeb, AIP Conference Proceedings, 2475, 9-18, (2023).
33. A. M. A. A.-S. T. A.A. Hassan, "Growth of Different Zinc Oxide Nanostructures for Hydrogen Gas Sensing," J. Glob. Pharma Technol., vol. 11, no. 02, pp. 419–425, 2019.
34. Kejeen M. Ibrahim, Wasan R. Saleh and , Abdulkareem M.A. Al-Sammarraie," Structural and Optical Properties of ZnO Nanostructures Synthesized by Hydrothermal Method at Different Conditions', Nano Hybrids and Composites,Vol. 35, pp 75-83, (2022).
35. S. Ananthakumar, J. Ramkumar, and S. Moorthy Babu. "Facile synthesis and transformation of Te nanorods to CdTe nanoparticles." Materials science in semiconductor processing, Vol.27, pp. (12-18), (2014).
36. Ramachandran, R., Saranya, M., Kollu, P., Raghupathy, B. P., Jeong, S. K., & Grace, A. N. Solvothermal synthesis of Zinc sulfide decorated Graphene (ZnS/G) nanocomposites for novel Supercapacitor electrodes. Electrochimica Acta, 178, 647-657, (2015).
37. H. Kim, C. M. Gilmore, A. Pique, J. S. Horwitz, H. Mattoussi, H. Murata, Z. H. Kafafi, and D. B. Chrisey, Electrical, optical, and structural properties of indium–tin–oxide thin films for organic light-emitting devices, Journal of applied physics, 86(11), 6451- 6461(1999)
38. A. Ponzoni, C. Baratto, N. Cattabiani, M. Falasconi, V. Galstyan, E. Nunez-Carmona, F. Rigoni, V. Sberveglieri, G. Zambotti, D. Zappa, Sensors, 17, 714 (2017).
39. A. N. Naje and W. k . Mahmood, "Sensitivity Performance of Single Wall Carbon Nanotubes Gas Sensor on Silicon and Porous Silicon", Materials Science and Engineering, vol. 454, Dec. 2018.
40. P. Sun, X. Zhou, C. Wang, B. Wang, X. Xu, and G. Lu, One-step synthesis and gas sensing properties of hierarchical Cd-doped SnO2 nanostructures, Sensors Actuators B: Chemical, 190, 32–39 (2014)